Acta Mech 215, 119–134 (2010)
DOI 10.1007/s00707-010-0327-4

Jun-Hong Guo · Zi-Xing Lu · Xiang Feng

The fracture behavior of multiple cracks emanating from a circular hole in piezoelectric materials

Received: 24 September 2009 / Revised: 28 February 2010 / Published online: 21 May 2010

Abstract Using the complex variable method and a new conformal mapping, the fracture behavior of multiple cracks emanating from a circular hole in piezoelectric materials is considered under remotely uniform in-plane electric and anti-plane mechanical loadings. The analytic solutions of the field intensity factors and the energy release rate are presented by taking the effect of dielectric permittivity into consideration. Known results can be derived as special cases from the general solutions. The results are illustrated with plots, showing that the piezoelectric material containing three radial cracks spaced equally at 120° apart originating from a circular hole is the easiest to fail for all cases of cracks originating from a circular hole under in-plane electric and anti-plane mechanical loadings. Moreover, if there exist multiple cracks ($n \geq 3$) originating from a circular hole in piezoelectric materials, an increase in the number of cracks can enhance the reliability of these materials. The star-shaped cracks possess similar characteristics.

1 Introduction

Piezoelectric materials have received considerable attention due to their use in monitoring and controlling structural components. Such materials show coupling effects between electric fields and elastic response. However, the brittle nature of piezoelectric materials easily leads to cracking or generating defects during the materials processing, manufacturing and when subjected to the strong electro-mechanical loading. In recent years, extensive research of piezoelectric materials with cracks has been carried out due to the practical importance [1–21]. The theoretical fundamentals of linear piezoelectric crack analysis are well documented in the review article written by Kuna [22] including original literature cited therein. So far, investigations have been confined to relatively simple and classical cracks. As we know, the holed structures play an important role in engineering, and cracks often exist around holes during manufacture and service of the holed structures. On the other hand, when piezoelectric materials are subjected to mechanical and electric loadings in service, the stress concentrations near the holes can induce crack initiation and propagation, which will lead to the failure of these piezoelectric materials. Therefore, it is necessary and important to analyze the fracture behavior of piezoelectric materials, especially when cracks emanating from holes are involved. Recently, Wang and Gao [16] solved the two symmetrical cracks and a single crack originating from the edge of a circular hole in a piezoelectric solid by introducing conformal mapping [23], and presented the exact solutions of the field intensity factors and the energy release rate. By developing new conformal mapping, Guo et al. [21] treated the two asymmetrical edge cracks emanating from an elliptical hole in a piezoelectric material and obtained the exact solutions of the field intensity factors and the energy release rate.

J.-H. Guo · Z.-X. Lu (✉) · X. Feng
Institute of Solid Mechanics, Beijing University of Aeronautics and Astronautics,
Beijing 100191, People's Republic of China
E-mail: luzixing@buaa.edu.cn
Tel.: +86-10-82317507
Fax: +86-10-82328501

However, for the case of multiple cracks at the edge of a circular hole, to the authors' knowledge the corresponding research is rather lacking in piezoelectric materials. For isotropic materials, Tada et al. [24], Ouchierlony [25], Wu and Carlsson [26] solved the multiple cracks originating from a circular hole under bidirectional tension and only obtained the numerical solutions of the stress intensity factor. But for the anti-plane problem, no analytical solutions of multiple cracks originating from a circular hole have been presented until now, which can be mainly attributed to the mathematical obstacles. Therefore, it is the aim of this work to study the fracture behavior and correlation of multiple cracks at the edge of a circular hole in piezoelectric materials. Furthermore, it is very interesting and challenging to present the analytical solutions for such complicated crack problems, since these solutions can provide the theoretical analysis for fracture problems in piezoelectric materials, and can also serve as a benchmark for the purpose of judging the accuracy and efficiency of various numerical and approximate methods.

In fracture analysis of piezoelectric materials, two kinds of electric boundary conditions, known as the electrically impermeable crack and electrically permeable crack, are common used on crack faces. In fact, they are two extreme cases of a real crack [27,28]. Indeed the crack opens under applied mechanical-electric loadings, while the electric field in the crack cavity significantly depends on the crack opening and the permeability of the material in the crack cavity. In this regard, the crack opening model [10] that considers the electric field in the crack cavity and is sometimes called the semi-permeable crack [27] is thought to be most appropriate to the facts. By taking the effect of dielectric permittivity into consideration, various electro-elastic behaviors of a dielectric crack have been reported by many researchers [13,29–36].

Up to now, only the problems of two symmetrical cracks originating from the edge of a circular hole [16] and two asymmetrical cracks emanating from an elliptical hole [21] in piezoelectric materials have been studied under the electrically impermeable assumption. For the exact electric boundary condition, however, the corresponding problems in piezoelectric materials have not been considered in previous studies due to the mathematical difficulty. It is therefore the objective of this work to study the fracture behavior of multiple cracks at the edge of a circular hole in a transversely isotropic piezoelectric solid by taking the effect of dielectric permittivity into consideration. A new and exact conformal mapping is developed to reduce the problem to the solution of Cauchy integral equations, and furthermore the analytic expressions of the field intensity factors and the energy release rate are derived. A comparison with the finite element method is made to confirm the correctness of the present solutions. Numerical examples are provided to show the effects of the ratio of crack length to hole-radius, the number of cracks and combined mechanical and electric loadings on the field intensity factors and the energy release rate. Some useful conclusions that play an important role in fracture analysis and structural design in engineering are drawn.

2 Basic formulation

In a Cartesian coordinate system $x_i (i = 1, 2, 3)$, the complete set of basic equations for a linear piezoelectric solid is [40]

$$\sigma_{ij} = C_{ijkl}\gamma_{kl} - e_{lij}E_l, \quad D_i = e_{ikl}\gamma_{kl} + \varepsilon_{il}E_l, \tag{1}$$

$$\sigma_{ij,j} = 0, \quad D_{i,i} = 0, \tag{2}$$

$$\gamma_{ij} = (u_{i,j} + u_{j,i})/2, \quad E_i = -\varphi_{,i}, \tag{3}$$

where a comma in the subscripts stands for a partial differentiation; the repeated indices denote summation; σ_{ij}, γ_{ij}, u_i, φ, D_i, E_i are the stress, the strain, the displacement, the electric potential, the electric displacement and the electric field, respectively, and C_{ijkl}, e_{lij} and ε_{il} stand for the elastic constants, the piezoelectric constants and the dielectric permittivity, respectively.

Solutions of the anti-plane problem are relatively simple and can be written in an explicit and closed-form, thereby easily providing physical insights into the fracture behavior of piezoelectric materials [13]. This paper is concerned with the electro-elastic problem of a mode III crack in the isotropic plane. Let a transversely isotropic piezoelectric solid with the poling direction along the positive x_3 axis and the isotropic plane in the x_1–x_2 plane. The anti-plane deformation is determined by the out-of-plane displacement and the in-plane electric field, and both are functions of x_1 and x_2, i.e.,

$$u_1 = u_2 = 0, \quad u_3 = u_3(x_1, x_2), \quad \varphi = \varphi(x_1, x_2). \tag{4}$$

Substituting Eq. (4) into Eq. (1) reduces to

$$\sigma_{3k} = c_{44}u_{3,k} + e_{15}\varphi_{,k}, \quad D_k = e_{15}u_{3,k} - \varepsilon_{11}\varphi_{,k}, \quad (k = 1,\ 2). \tag{5}$$

Furthermore, inserting Eqs. (4) and (5) into Eq. (2) leads to

$$\mathbf{B}_0 \nabla^2 \mathbf{u} = \mathbf{0}, \tag{6}$$

where $\nabla^2 = \partial^2/\partial x_1^2 + \partial^2/\partial x_2^2$ and

$$\mathbf{u} = [u_3, \varphi]^{\mathrm{T}}, \quad \mathbf{B}_0 = \begin{bmatrix} c_{44} & e_{15} \\ e_{15} & -\varepsilon_{11} \end{bmatrix}, \tag{7}$$

where the superscript T represents the transpose.

Since $\mathbf{B}_0$ is non-singular, Eq. (6) becomes

$$\nabla^2 \mathbf{u} = \mathbf{0}. \tag{8}$$

Similarly, we introduce a generalized stress function vector $\boldsymbol{\phi}$, such that

$$[\sigma_{31}, D_1]^{\mathrm{T}} = -\boldsymbol{\phi}_{,2}, \quad [\sigma_{32}, D_2]^{\mathrm{T}} = \boldsymbol{\phi}_{,1}. \tag{9}$$

The general solutions of Eqs. (8) and (9) can be expressed by the generalized displacement $\mathbf{u}$ and the stress function $\boldsymbol{\phi}$, as [13]

$$\mathbf{u} = \mathbf{A}\mathbf{f}(z) + \overline{\mathbf{A}\mathbf{f}(z)}, \tag{10}$$

$$\boldsymbol{\phi} = \mathbf{B}\mathbf{f}(z) + \overline{\mathbf{B}\mathbf{f}(z)}, \tag{11}$$

where $\mathbf{f}(z)$ is an unknown complex vector; the overbar stands for the conjugate of a complex number; $\mathbf{A}$ and $\mathbf{B}$ stand for the material constant matrices defined as

$$\mathbf{A} = \mathbf{I}, \quad \mathbf{B} = \mathrm{i}\mathbf{B}_0, \tag{12}$$

where $\mathbf{I}$ is a 2×2 unit matrix.

If the complex potential $\mathbf{f}(z)$ is determined from boundary conditions, all the fields can be obtained by Eqs. (3) and (9).

Equations (10) and (11) can be rewritten as

$$\boldsymbol{\phi} = 2\mathrm{Re}[\mathbf{k}(z)], \tag{13}$$

$$\mathbf{u} = 2\mathrm{Im}[\mathbf{Y}\mathbf{k}(z)], \tag{14}$$

where

$$\mathbf{k}(z) = \mathbf{B}\mathbf{f}(z), \tag{15}$$

$$\mathbf{Y} = \mathrm{i}\mathbf{A}\mathbf{B}^{-1}. \tag{16}$$

From Eqs. (12) and (16), one finds

$$\mathbf{Y} = \mathbf{B}_0^{-1}. \tag{17}$$

Let us define

$$\mathbf{H} = 2\mathrm{Re}[\mathbf{Y}]. \tag{18}$$

Since $\mathbf{Y}$ is real in the current case, Eq. (18) becomes

$$\mathbf{H} = 2[\mathbf{Y}] = \frac{2}{\det \mathbf{B}_0} \begin{pmatrix} \varepsilon_{11} & e_{15} \\ e_{15} & -c_{44} \end{pmatrix}, \tag{19}$$

where

$$\det \mathbf{B}_0 = c_{44}\varepsilon_{11} + e_{15}^2. \tag{20}$$

3 Conformal mapping and analytic solutions

Consider multiple cracks at the edge of a circular hole in an infinite piezoelectric solid, as shown in Fig. 1. The solid is subjected to uniform remote out-plane shear and in-plane electric field loadings, i.e., $\Sigma_{2\infty} = [\sigma_{32}^{\infty}, D_2^{\infty}]^{\mathrm{T}}$ and $\Sigma_{1\infty} = [\sigma_{31}^{\infty}, D_1^{\infty}]^{\mathrm{T}}$. The hole and cracks are free of traction on their surfaces and are filled with air of a dielectric permittivity, ε_0. Using the technique of conformal mapping and complex variable method, we study the complex potentials, the field intensity factors and the energy release rate under different combinations of electric and mechanical loadings at infinity as follows.

3.1 Conformal mapping function

As we know, many studies indicate that two commonly used electric boundary conditions, i.e., electrically permeable model and electrically impermeable model, can be taken as two limiting cases of the realistic crack. This is because for a realistic crack full of medium (usually air or vacuum), the dielectric permittivity of the crack interior does not vanish although it is very small. Besides, due to the existence of the medium inside the crack or hole, the electric potentials are discontinuous. For example, the evidence that an electric potential has a jump across the crack faces for a poled PZT ceramic has been observed in experiment [37]. Based on such considerations, in this paper we consider a more reasonable case or an intermediate state of the above two cases.

In this case, the electric field inside the circular hole and cracks is uniform, and the potential functions can be expressed as

$$\boldsymbol{\phi}_0 = \left(\lambda_e D_2^0 x_1 - D_1^0 x_2\right) \mathbf{i}_2, \tag{21}$$

$$\varphi_0 = -E_1^0 x_1 - \lambda_e E_2^0 x_2, \tag{22}$$

where $\mathbf{i}_2 = [0, 1]^{\mathrm{T}}$, and D_k^0 and E_k^0 are the components of the electric displacement and electric field inside the hole and the cracks for a fully permeable crack, respectively, which are constant and to be determined by the loading condition; the parameter λ_e is introduced to characterize the permeability of the electric field inside the cracks and hole, similar to the treatment in [38] and [39]. Generally speaking, λ_e is nonlinearly related to applied loadings as well as the permeability of the crack interior, and here for simplicity we take $\lambda_e \in [0, 1]$. The crack is impermeable if $\lambda_e = 0$, permeable if $\lambda_e = 1$, and semi-permeable if $\lambda_e \in (0, 1)$.

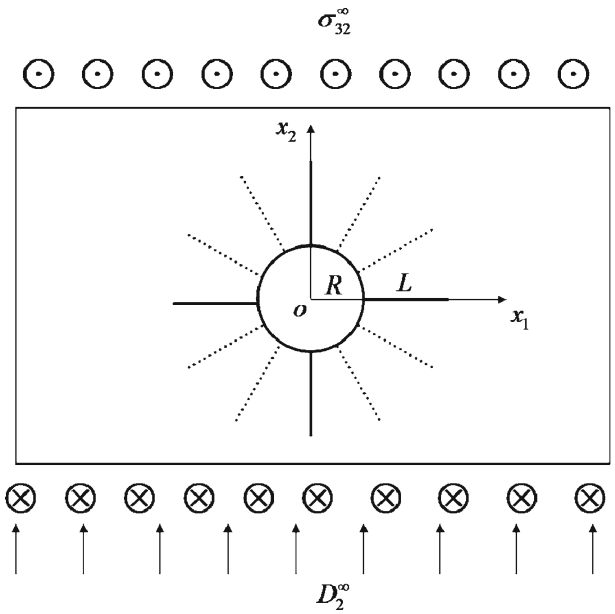

Fig. 1 Multiple cracks at the edge of a circular hole in an infinite piezoelectric solid

In the solid, the potential vector has the following form [13]:

$$\mathbf{f}(z) = \mathbf{c}^{\infty} z + \mathbf{f}_0(z), \tag{23}$$

where $\mathbf{c}^{\infty}$ is a complex constant related to the remote loading conditions, and $\mathbf{f}_0(z)$ is an unknown complex function that nulls at infinity, i.e., $\mathbf{f}_0(\infty) = \mathbf{0}$. Substituting Eq. (23) into Eqs. (13) and (14) and noting that $\mathbf{Y}$ is real, we have

$$\boldsymbol{\phi} = \Sigma_{2\infty} x_1 - \Sigma_{1\infty} x_2 + 2\mathrm{Re}[\mathbf{k}_0(z)], \tag{24}$$
$$\varphi = -E_1^{\infty} x_1 - E_2^{\infty} x_2 + 2\mathrm{Im}[\mathbf{Y}\mathbf{k}_0(z)]_2, \tag{25}$$

in which $[]_2$ denotes the 2nd row of the vector $[\ ]$ and $\mathbf{k}_0(z) = \mathbf{B}\mathbf{f}_0(z)$.

On the surfaces of the hole and cracks, the continuity conditions require

$$\boldsymbol{\phi} = \boldsymbol{\phi}_0, \quad \varphi = \varphi_0. \tag{26}$$

Substituting Eqs. (21), (22), (24) and (25) into Eq. (26) results in

$$\Sigma_{\lambda_e}^{2\infty} x_1 - \Sigma_{\lambda_e}^{1\infty} x_2 + 2\mathrm{Re}[\mathbf{k}_0(z)] = 0, \tag{27}$$
$$\left(E_1^{\infty} - E_1^0\right) x_1 + \left(E_2^{\infty} - \lambda_e E_2^0\right) x_2 - 2\mathrm{Im}[\mathbf{Y}\mathbf{k}_0(z)]_2 = 0, \tag{28}$$

where

$$\Sigma_{\lambda_e}^{2\infty} = \left[\sigma_{32}^{\infty}, D_2^{\infty} - \lambda_e D_2^0\right]^{\mathrm{T}}, \quad \Sigma_{\lambda_e}^{1\infty} = \left[\sigma_{31}^{\infty}, D_1^{\infty} - D_1^0\right]^{\mathrm{T}}. \tag{29}$$

The above boundary value problems will be solved by the following method, which is different from the previous work [13]. Equations (27) and (28) can be expressed as

$$\Sigma_{\lambda_e}^{2\infty}\mathrm{Re}[z] - \Sigma_{\lambda_e}^{1\infty}\mathrm{Im}[z] + 2\mathrm{Re}[\mathbf{k}_0(z)] = 0, \tag{30}$$
$$\left(E_1^{\infty} - E_1^0\right)\mathrm{Re}[z] + \left(E_2^{\infty} - \lambda_e E_2^0\right)\mathrm{Im}[z] - 2\mathrm{Im}[\mathbf{Y}\mathbf{k}_0(z)]_2 = 0. \tag{31}$$

Consequently, Eqs. (30) and (31) become the following expressions:

$$\frac{1}{2}\Sigma_{\lambda_e}^{2\infty}(z+\overline{z}) + \frac{\mathrm{i}}{2}\Sigma_{\lambda_e}^{1\infty}(z-\overline{z}) + 2\mathrm{Re}[\mathbf{k}_0(z)] = 0, \tag{32}$$
$$\frac{1}{2}\left(E_1^{\infty} - E_1^0\right)(z+\overline{z}) - \frac{\mathrm{i}}{2}\left(E_2^{\infty} - \lambda_e E_2^0\right)(z-\overline{z}) - 2\mathrm{Im}\left[\mathbf{Y}\mathbf{k}_0(z)\right]_2 = 0. \tag{33}$$

To solve the boundary-value problem, it is convenient to utilize the technique of the conformal mapping, which can transform the problem in the z plane to Cauchy integral equations in the ζ plane, and the closed-form solutions are further obtainable. Wang and Gao [16] obtained the exact solutions of two cracks and a single crack issued from a circular hole by introducing the conformal mapping [23]. However, the conformal mapping presented in a series form was complicated. Researches on simpler and efficient methods for resolving more complicated problems are still a necessary and important task for fracture mechanics. In this work, to study the fracture behavior of multiple cracks at the edge of a circular hole, we propose a new conform mapping as follows:

$$z = \omega(\zeta) = R2^{-\frac{2}{n}}\zeta^{-1}\left[\varepsilon(\zeta^n + 1) + \sqrt{\varepsilon^2(\zeta^n+1)^2 - 4\zeta^n}\right]^{\frac{2}{n}}, \tag{34}$$

where n denotes the number of cracks, and

$$\varepsilon = \frac{1}{2}\left[(1+\lambda)^{\frac{n}{2}} + (1+\lambda)^{-\frac{n}{2}}\right], \quad \lambda = L/R. \tag{35}$$

It can be shown that Eq. (34) provides a conformal mapping from the outside region of the hole and cracks in the physical plane to the interior of a unit circle in the ζ plane, and $z = R + L = \omega(1)$.

In the ζ plane, Eqs. (32) and (33) can be transformed into

$$\frac{1}{2}\mathbf{\Sigma}_{\lambda_e}^{2\infty}\left(\omega(\sigma)+\overline{\omega(\sigma)}\right)+\frac{\mathrm{i}}{2}\mathbf{\Sigma}_{\lambda_e}^{1\infty}\left(\omega(\sigma)-\overline{\omega(\sigma)}\right)+2\mathrm{Re}[\mathbf{k}_0(\sigma)]=0, \tag{36}$$

$$\frac{1}{2}\left(E_1^{\infty}-E_1^0\right)\left(\omega(\sigma)+\overline{\omega(\sigma)}\right)-\frac{\mathrm{i}}{2}(E_2^{\infty}-\lambda_e E_2^0)\left(\omega(\sigma)-\overline{\omega(\sigma)}\right)-2\mathrm{Im}[\mathbf{Y}\mathbf{k}_0(\sigma)]_2=0, \tag{37}$$

where $\sigma=e^{\mathrm{i}\theta}$ is the point on the unit circle, and $\mathbf{f}_0(\sigma)=\mathbf{f}_0(\omega(\sigma))$ is defined. It can be found from Eq. (34) that $\overline{\omega(\sigma)}=\omega(\sigma)$. Thus, Eqs. (36) and (37) can be simplified as

$$\Sigma_{\lambda_e}^{2\infty}\omega(\sigma)+\mathbf{B}\mathbf{f}_0(\sigma)+\overline{\mathbf{B}\mathbf{f}_0(\sigma)}=0, \tag{38}$$

$$\left(E_1^{\infty}-E_1^0\right)\omega(\sigma)+\mathrm{i}\left[\mathbf{Y}\mathbf{k}_0(\sigma)-\overline{\mathbf{Y}\mathbf{k}_0(\sigma)}\right]_2=0. \tag{39}$$

Multiplying the resultant equation by $\mathrm{d}\sigma/[2\pi\mathrm{i}(\sigma-\zeta)]$, where ζ is a point inside of the unit circle, and performing the Cauchy integration on the unit circle τ in the clockwise direction, Eqs. (38) and (39) yield

$$\Sigma_{\lambda_e}^{2\infty}\frac{1}{2\pi\mathrm{i}}\int_{\tau}\frac{\omega(\sigma)}{\sigma-\zeta}\mathrm{d}\sigma+\frac{1}{2\pi\mathrm{i}}\int_{\tau}\frac{\mathbf{B}\mathbf{f}_0(\sigma)}{\sigma-\zeta}\mathrm{d}\sigma+\frac{1}{2\pi\mathrm{i}}\int_{\tau}\frac{\overline{\mathbf{B}\mathbf{f}_0(\sigma)}}{\sigma-\zeta}\mathrm{d}\sigma=0, \tag{40}$$

$$\left(E_1^{\infty}-E_1^0\right)\frac{1}{2\pi\mathrm{i}}\int_{\tau}\frac{\omega(\sigma)}{\sigma-\zeta}\mathrm{d}\sigma+\mathrm{i}\frac{1}{2\pi\mathrm{i}}\int_{\tau}\frac{\left[\mathbf{Y}\mathbf{k}_0(\sigma)-\overline{\mathbf{Y}\mathbf{k}_0(\sigma)}\right]_2}{\sigma-\zeta}\mathrm{d}\sigma=0. \tag{41}$$

Since $\mathbf{f}_0(\zeta)$ is analytic in the interior region of the unit circle, for an arbitrary point in $\{\zeta\,||\zeta|<1\}$, we have from Eqs. (40) and (41), that

$$\mathbf{B}\mathbf{f}_0(\zeta)=-\Sigma_{\lambda_e}^{2\infty}\frac{1}{2\pi\mathrm{i}}\int_{\tau}\frac{\omega(\sigma)}{\sigma-\zeta}\mathrm{d}\sigma, \tag{42}$$

$$\mathrm{i}[\mathbf{Y}\mathbf{k}_0(\zeta)]_2=-\left(E_1^{\infty}-E_1^0\right)\frac{1}{2\pi\mathrm{i}}\int_{\tau}\frac{\omega(\sigma)}{\sigma-\zeta}\mathrm{d}\sigma. \tag{43}$$

It is found from Eq. (34) that $\omega(\sigma)$ is the boundary value of the analytic function $\omega(\zeta)$ inside the unit circle τ except the point $\zeta=0$. By the Residue theorem, we have

$$\frac{1}{2\pi\mathrm{i}}\int_{\tau}\frac{\omega(\sigma)}{\sigma-\zeta}d\sigma=\omega(\zeta)-\frac{1}{\zeta}R\varepsilon^{\frac{2}{n}}. \tag{44}$$

Substituting Eq. (44) into Eqs. (42) and (43) and differentiating them with respect to ζ leads to

$$\mathbf{B}\mathbf{F}_0(\zeta)=-\Sigma_{\lambda_e}^{2\infty}\left[\omega'(\zeta)+\frac{1}{\zeta^2}R\varepsilon^{\frac{2}{n}}\right], \tag{45}$$

$$\mathrm{i}[\mathbf{Y}\mathbf{B}\mathbf{F}_0(\zeta)]_2=-\left(E_1^{\infty}-E_1^0\right)\left[\omega'(\zeta)+\frac{1}{\zeta^2}R\varepsilon^{\frac{2}{n}}\right], \tag{46}$$

where $\mathbf{F}_0(\zeta)=\mathrm{d}\mathbf{f}_0(\zeta)/\mathrm{d}\zeta$, and $\omega'(\zeta)$ can be obtained from Eq. (34) as

$$\omega'(\zeta)=2^{-\frac{2}{n}}R\zeta^{-2}\left[\varepsilon(\zeta^n+1)+S\right]^{\frac{2}{n}-1}\left[\varepsilon+\varepsilon^2(\zeta^n+1)/S\right](\zeta^n-1), \tag{47}$$

where

$$S=\sqrt{\varepsilon^2(\zeta^n+1)^2-4\zeta^n}. \tag{48}$$

Inserting Eq. (45) into Eq. (46) and using Eqs. (19) and (29), one finds

$$E_1^{\infty} = E_1^0, \tag{49}$$

$$D_2^{\infty} - \lambda_e D_2^0 = \frac{e_{15}}{c_{44}} \sigma_{32}^{\infty}. \tag{50}$$

Consequently, the electric displacement components inside the circular hole and cracks are obtained as

$$D_1^0 = \varepsilon_0 E_1^{\infty}, \tag{51}$$

$$D_2^{\infty} - D_2^0 = -(1 - \lambda_e) D_2^0 + \frac{e_{15}}{c_{44}} \sigma_{32}^{\infty}. \tag{52}$$

Equations (51) and (52) show that the component of the electric displacement D_1^0 is independent of the permeability of the crack, but the component of the electric displacement D_2^0 is related to the permeability λ_e of the electric field. The same conclusion can be found in the previous study [13]. For the electrically impermeable crack, $D_2^0 = 0$; for a permeable crack, $\lambda_e = 1$, one has from Eq. (52) that

$$D_2^{\infty} - D_2^0 = \frac{e_{15}}{c_{44}} \sigma_{32}^{\infty}. \tag{53}$$

3.2 Field intensity factors

The vector of the field intensity factors can be expressed in the ζ-plane as [16]

$$\boldsymbol{\kappa} = (k_\sigma, k_D)^T = 2\sqrt{\pi} \lim_{\zeta \to 1} \frac{\mathbf{BF}_0(\zeta)}{\sqrt{\omega''(\zeta)}} = 2\sqrt{\pi} \frac{\mathbf{BF}_0(1)}{\sqrt{\omega''(1)}}. \tag{54}$$

From Eq. (47), $\omega''(1)$ can be derived as

$$\omega''(1) = \frac{1}{2} Rn\varepsilon \left(\varepsilon + \sqrt{\varepsilon^2 - 1}\right)^{\frac{2}{n}} \left(\varepsilon^2 - 1\right)^{-\frac{1}{2}}. \tag{55}$$

Inserting Eqs. (45) and (55) into Eq. (54), and noting Eqs. (18) and (29), one finally has

$$\boldsymbol{\kappa} = K\sqrt{\pi L} \left[\sigma_{32}^{\infty}, D_2^{\infty} - \lambda_e D_2^0\right]^{\mathrm{T}}, \tag{56}$$

in which K, called the dimensionless intensity factor, is defined as

$$K = 2^{\frac{3n-4}{2n}} n^{-\frac{1}{2}} \lambda^{-\frac{1}{2}} [(1+\lambda)^n + 1]^{\frac{4-n}{2n}} [(1+\lambda)^n - 1]^{\frac{1}{2}} (1+\lambda)^{-\frac{3}{2}}, \tag{57}$$

where λ is given by Eq. (35). In particular, when R tends to zero, i.e., $\lambda \to \infty$, Eq. (57) reduces to

$$K = 2^{\frac{3n-4}{2n}} n^{-\frac{1}{2}}. \tag{58}$$

This is the case of n equal and equally spaced radial cracks emanating from a common point, which is consistent with the classical result [24,41] with respect to the stress intensity factor.

Using Eq. (53), Eq. (56) can be further written as

$$k_\sigma = \sigma_{32}^{\infty} K\sqrt{\pi L}, \tag{59}$$

$$k_D = \left[(1 - \lambda_e) D_2^{\infty} + \lambda_e \frac{e_{15}}{c_{44}} \sigma_{32}^{\infty}\right] K\sqrt{\pi L}. \tag{60}$$

Equations (59) and (60) indicate that the stress intensity factor is independent of the permeability of the electric field λ_e. However, the electric displacement intensity factor is a function of λ_e. For an impermeable crack, $\lambda_e = 0$ and Eq. (60) can be reduced to

$$k_D = D_2^{\infty} K\sqrt{\pi L}. \tag{61}$$

For a permeable crack, $\lambda_e = 1$, and combining Eqs. (59) and (60) gives

$$k_D = \frac{e_{15}}{c_{44}} \sigma_{32}^{\infty} K\sqrt{\pi L} = \frac{e_{15}}{c_{44}} k_\sigma. \tag{62}$$

Equation (62) shows that the electric displacement intensity factor is induced by the piezoelectric effect for a permeable crack. The same conclusions are also presented by Zhang and Gao [13].

3.3 Energy release rate

The energy release rate is a significant parameter for the study of failure analysis of piezoelectric materials. Based on a path-independent integral for a cracked piezoelectric material [42], the energy release rate can be expressed as

$$G = \frac{1}{4}\boldsymbol{\kappa}^{\mathrm{T}}\mathbf{H}\boldsymbol{\kappa}. \tag{63}$$

Substituting Eqs. (19) and (56) into Eq. (63) reduces to

$$G = \frac{K^2\pi L}{2\left(c_{44}\varepsilon_{11}+e_{15}^2\right)}\left\{\varepsilon_{11}\sigma_{32}^{\infty 2}+2e_{15}\sigma_{32}^{\infty}\left[(1-\lambda_e)D_2^{\infty}+\lambda_e\frac{e_{15}}{c_{44}}\sigma_{32}^{\infty}\right]-c_{44}\left[(1-\lambda_e)D_2^{\infty}+\lambda_e\frac{e_{15}}{c_{44}}\sigma_{32}^{\infty}\right]^2\right\}. \tag{64}$$

Equation (64) shows that the energy release rate of multiple cracks emanating from a circular hole is dependent on the electric loading, mechanical loading, material constants, permeability of the electric field λ_e and the dimensionless intensity factor.

For an impermeable crack, $\lambda_e = 0$, we have from Eq. (64) that

$$G = \frac{K^2\pi L}{2\left(c_{44}\varepsilon_{11}+e_{15}^2\right)}\left(\varepsilon_{11}\sigma_{32}^{\infty 2}+2e_{15}\sigma_{32}^{\infty}D_2^{\infty}-c_{44}D_2^{\infty 2}\right). \tag{65}$$

On the other hand, for a permeable crack, $\lambda_e = 1$, Eq. (64) becomes

$$G = \frac{K^2\pi L}{2c_{44}}\sigma_{32}^{\infty 2}. \tag{66}$$

4 Special cases and numerical examples

4.1 Several special cases

The dimensionless intensity factor, K, can be used to determine the field intensity factors and the energy release rate of multiple cracks emanating from a circular hole. Some special cases for the field intensity factors and the energy release rate of the present results are discussed as follows.

When $n = 1$, Eq. (57) then reduces to

$$K = 2^{-\frac{1}{2}}(2+\lambda)^{\frac{3}{2}}(1+\lambda)^{-\frac{3}{2}}. \tag{67}$$

Equation (67) shows the case of a single edge crack emanating from a circular hole, which is identical to the result given by [16,21]. Especially, Eq. (67) can be degenerated into the result of a central crack in an infinite piezoelectric solid, i.e., $K = 1/\sqrt{2}$, when R tends to zero.

When $n = 2$, then Eq. (57) leads to

$$K = \lambda^{-\frac{1}{2}}\left[(\lambda+1)^4-1\right]^{\frac{1}{2}}(\lambda+1)^{-\frac{3}{2}}. \tag{68}$$

This is just the result of two symmetrical edge cracks originating from a circular hole, which is shown to be in excellent agreement with the corresponding result presented in [16,21]. In addition, the stress intensity factor agrees well with that of isotropic materials [41] in the absence of the electric load at infinity. In particular, Eq. (68) reduces to the result of the Griffith crack, i.e., $K = 1$, when R approaches to zero, which is expectable.

When $n = 3$, from Eq. (57) it follows that

$$K = 2^{\frac{5}{6}}3^{-\frac{1}{2}}\lambda^{-\frac{1}{2}}\left[(1+\lambda)^3+1\right]^{\frac{1}{6}}\left[(1+\lambda)^3-1\right]^{\frac{1}{2}}(1+\lambda)^{-\frac{3}{2}}. \tag{69}$$

Equation (69) gives the result of three radial cracks spaced equally at 120° apart originating from a circular hole. Especially, when R tends to zero, Eq. (69) gives

$$K = 2^{\frac{5}{6}}3^{-\frac{1}{2}}, \tag{70}$$

which is the case of three radial cracks spaced equally at 120° apart originating from a common point.

When $n = 4$, from Eq. (57), we have

$$K = \lambda^{-\frac{1}{2}} \left[(\lambda + 1)^4 - 1\right]^{\frac{1}{2}} (\lambda + 1)^{-\frac{3}{2}}, \tag{71}$$

which is the result of four radial cracks emanating from a circular hole. From Eqs. (68) and (71), it is interesting to note that the result of two radial cracks emanating from a circular hole is the same as that of four radial cracks in a piezoelectric solid. This result indicates that if the piezoelectric solid containing four radial cracks originating from a circular hole is subjected to uniform loading along the y-axis or z-axis direction, the existence of the perpendicular crack has no effect on the field intensity factors and the energy release rate at the crack tip of the horizontal crack due to its geometrical symmetry. In particular, when R tends to zero, Eq. (71) reduces to the result of a cross-shaped crack [21], i.e., $K = 1$.

The energy release rate of special models mentioned earlier at the crack tip can be obtained by replacing K in Eqs. (64)–(66) with K derived from Eqs. (67)–(71).

4.2 Numerical examples

To illustrate the singular electro-elastic fields at the tip of the crack, numerical examples for a cracked PZT-5H piezoelectric ceramic are given, the material properties of which are [42] $c_{44} = 3.53 \times 10^{10}$ N/m^2, $e_{15} = 17.0$ C/m^2, $\varepsilon_{11} = 151 \times 10^{-10}$ C/Vm and $G_{\mathrm{cr}} = 5.0$ N/m, where G_{cr} is the critical energy release rate.

Figure 2 is devoted to the effects of the ratio of crack length to hole-radius on the dimensionless intensity factor K for the cases of $n = 1,\ 2,\ 3,\ 4$. It is seen that the value of K decreases as the ratio of L/R increases, and it is close to constant as the value of L/R tends to infinity. Figure 3 shows the variation of K with the number of cracks n. It is interesting to note that the value of K for the case of $n = 3$ is the largest one of all the cases of n. Moreover, the value of K for the case of $n = 2$ which equals that of $n = 4$ is larger than that for the case of $n = 1$. The value of K then further decreases as the number of cracks increases with $n \geq 5$. From the interesting phenomenon, several important and meaningful conclusions can be drawn: (i) The piezoelectric material containing the defect such as three radial cracks spaced equally at 120° apart originating from a circular hole will easier fail than the other cases under anti-plane shear loading. (ii) The piezoelectric material containing two cracks or four cracks emanating from a circular hole is easier to fail than the material with a single crack originating from a circular hole, which has been also pointed out by Guo et al. [21]. (iii) Once the multiple cracks ($n \geq 3$) at the edge of a circular hole occur in a piezoelectric material, an increase in the number of cracks can enhance the reliability of this material. In particular, the dimensionless intensity factors are close to zero when the number of cracks tends to infinity. This is because the boundary of multiple cracks originating from a circular hole is regarded as a new circular hole which is bigger

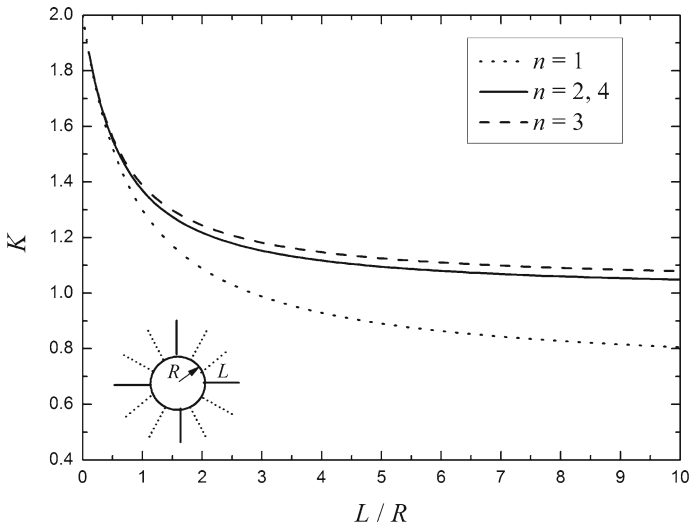

Fig. 2 Variation of the dimensionless intensity factor K with the ratio L/R

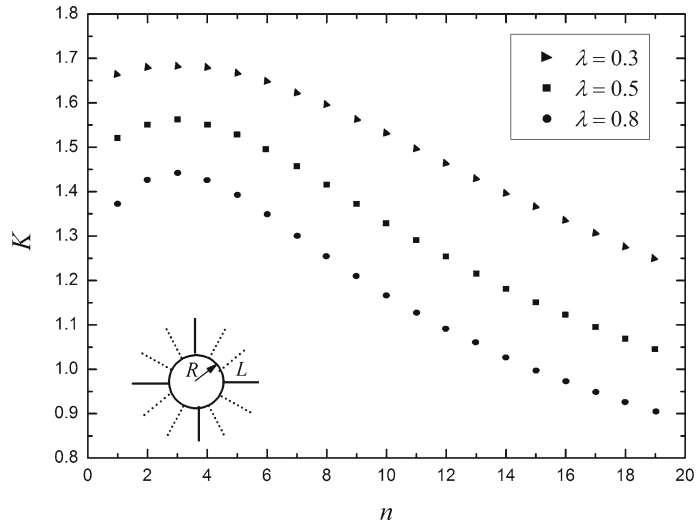

Fig. 3 Variation of K with the number of cracks n

Table 1 A comparison between the finite element (FE) results of the dimensionless stress intensity factors $K^* = K_\sigma/(\sigma_{32}^\infty\sqrt{L})$ and the present solutions for $\sigma_{32}^\infty = 3$ MPa, $R = 0.005$ m, $L = 0.0025$ m

Crack number n	FE results	Analytic solutions	Errors (%)
1	2.66835	2.69670	1.05
2	2.72125	2.75011	1.05
3	2.72976	2.76638	1.32
4	2.70519	2.75011	1.63
5	2.67966	2.70863	1.07
6	2.62763	2.64983	0.84

Table 2 A comparison between the finite element (FE) results of the dimensionless stress intensity factors K^* and the present solutions for $\sigma_{32}^\infty = 3$ MPa, $R = 0.005$ m, $L = 0.01$ m

Crack number n	FE results	Analytic solutions	Errors (%)
1	1.9335	1.9296	0.20
2	2.20119	2.15736	1.99
3	2.24012	2.20473	1.58
4	2.19109	2.15736	1.54
5	2.08290	2.07584	0.34
6	1.94904	1.98769	1.94

than the original one. To confirm the correctness of the obtained conclusions above, a comparison of the present solutions with the finite element results for the dimensionless stress intensity factors $K^* = K_\sigma/\left(\sigma_{32}^\infty\sqrt{L}\right)$ is listed in Table 1 ($\lambda = L/R = 1/2$) and Table 2 ($\lambda = L/R = 2$). It is seen that the finite element results are in good agreement with the present solutions for various values of n and λ. The variation of the dimensionless stress intensity factors K^* with the number of cracks n is plotted in Fig. 4. It is also observed that the trend of the curve obtained by the finite element method is the same as that of the present method. The numerical example shows the correctness of the present solutions, and these analytic solutions can also provide a benchmark for the purpose of judging the accuracy and efficiency of various numerical and approximate methods. It is pointed out that the resulting conclusions above should hold for other brittle materials.

For the case of multiple cracks originating from a circular hole of $R = 0.01$ m, the changes of the energy release rate with the length and the number of cracks are plotted under combined mechanical loading $\sigma_{32}^\infty = 6$ MPa and electric loading $D_2^\infty = 2\text{e} - 3$ C/m^2, as shown in Figs. 5 and 6, respectively. A permeable crack ($\lambda_e = 1$) gives the highest value of G/G_{cr}, while an impermeable crack ($\lambda_e = 0$) yields the lowest value of G/G_{cr}. It can be observed from Fig. 5 that the energy release rate of three radial cracks spaced equally at 120° apart originating from a circular hole increases as the crack length becomes longer, indicating that an

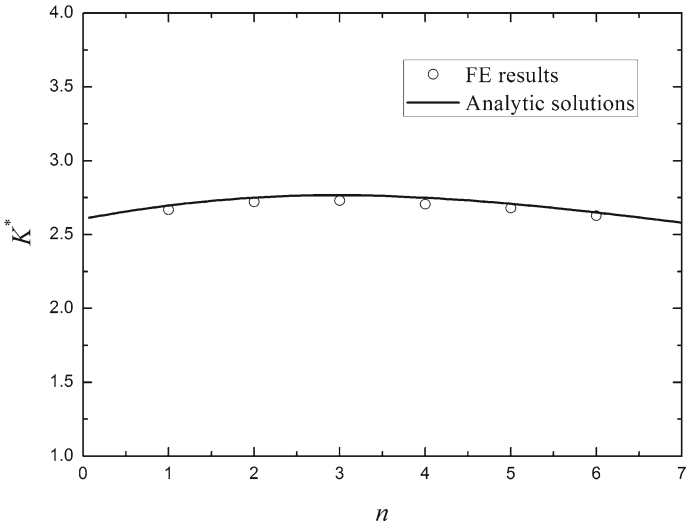

(a) $\lambda = 1/2$

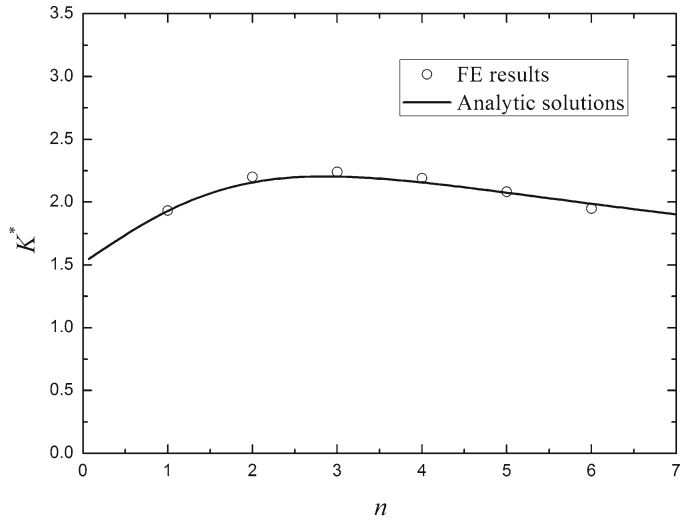

(b) $\lambda = 2$

Fig. 4 A comparison between the finite element (FE) results of the dimensionless stress intensity factors and the present solutions

increase in the crack length easily promotes the crack propagation. It is pointed out that the same conclusions hold for all other cases of n. The variation of the energy release rate with the number of cracks is shown in Fig. 6; similar conclusions can be drawn for the dimensionless intensity factor (Fig. 3).

Figures 7 and 8 show the effects of the applied mechanical and electrical loadings on the energy release rate for a given radius of $R = 0.01$ m and length of cracks $L = 0.005$ m, respectively. Without loss of generality, we take the case of $n = 3$ for example. The energy release rate $G/G_{\rm cr}$ is always positive under the applied pure mechanical load (Fig. 7). It can be found that the energy release rate rises rapidly as the applied mechanical load increases, suggesting that the applied mechanical load always promotes the crack growth. Figure 8 shows the variation of the energy release rate with the applied electric load under a given mechanical loading $\sigma_{32}^{\infty} = 6$ MPa. It is seen that for a given mechanical load the energy release rate of an impermeable crack or a semi-permeable crack decreases as the magnitude of the applied negative electric field increases. In contrast to that, the energy release rate increases as the applied positive electric field increases from zero, and reaches peak values at the same symmetric axis where $D_2^{\infty} = 2.89\text{e} - 3$ C/m^2. The energy release rate then continuously declines as the applied positive electric field further increases. However, for a permeable crack, the applied electric field has no effect on the energy release rate irrespective of the value

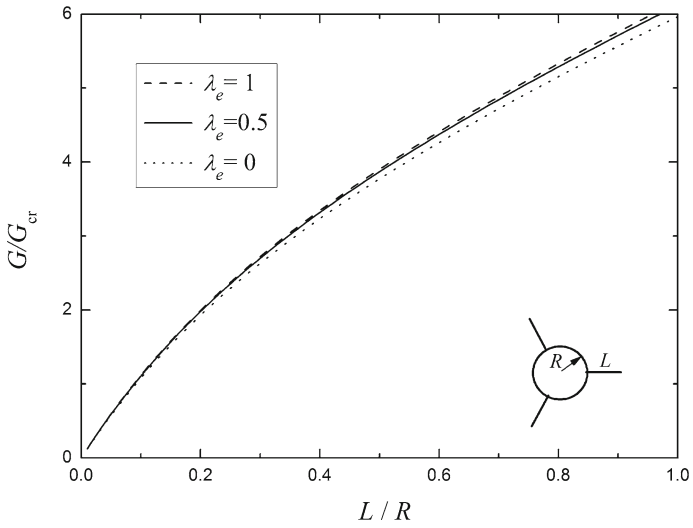

Fig. 5 Effect of the length of the crack on the energy release rate of three radial cracks spaced equally at 120° apart originating from a circular hole under combined mechanical loading $\sigma_{32}^{\infty} = 6$ MPa and electric loading $D_2^{\infty} = 2\text{e} - 3$ C/m^2

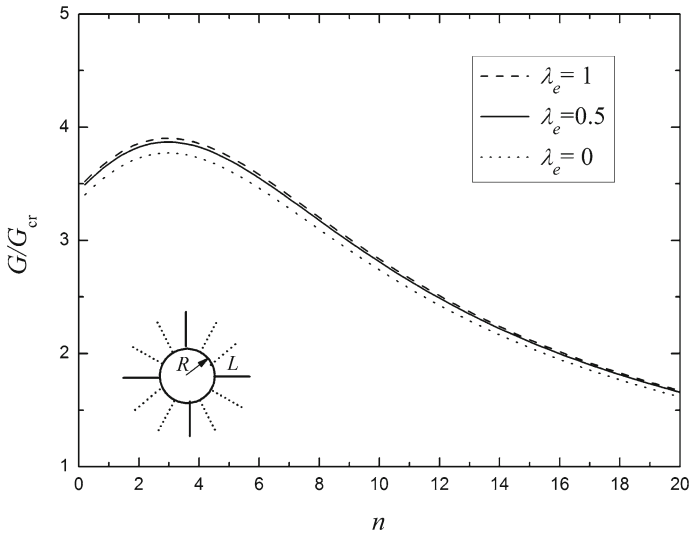

Fig. 6 Effect of the number of cracks on the energy release rate of multiple cracks emanating from a circular hole under combined mechanical loading $\sigma_{32}^{\infty} = 6$ MPa and electric loading $D_2^{\infty} = 2\text{e} - 3$ C/m^2

of applied mechanical loading. The results show that at a given mechanical load the negative electric field always retards crack growth, while the positive electric field can either enhance or retard crack propagation, which is dependent on the strengths of the applied electric field and the level of the mechanical load as well for an impermeable crack as a semi-permeable crack. For a permeable crack under combined mechanical and electric loadings, the energy release rate is dependent on only the mechanical loading. The same conclusions have been also obtained by [13,28,39]. Meanwhile, an experimental work [37] shows that an applied electric field always has a tendency to retard crack growth. An easily understandable picture about the negative energy release rate was proposed in [13].

Figure 9 exhibits the effects of the parameter λ_e, on the energy release rate ($n = 3$) for given the radius of $R = 0.01$ m and the length of cracks $L = 0.005$ m under a given mechanical loading $\sigma_{32}^{\infty} = 6$ MPa. It is seen that the influence of a negative electric field on the energy release rate is larger than that of a positive electric field. The result indicates that for a fixed mechanical loading a negative electric loading is generally prone to inhibit the crack extension rather than a positive one.

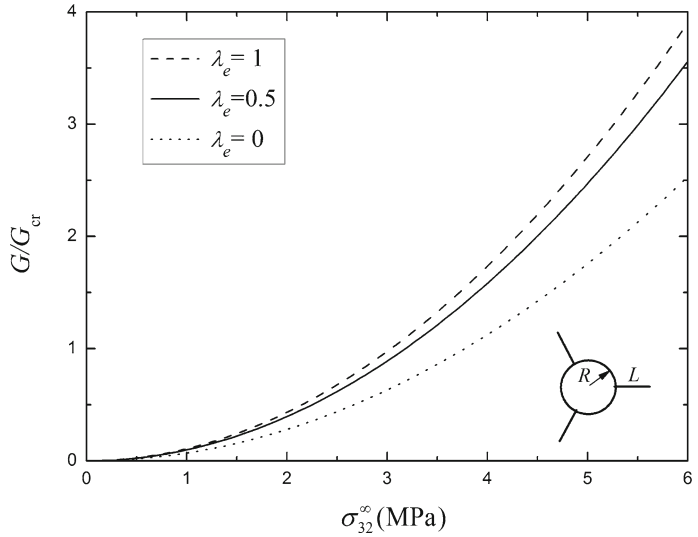

Fig. 7 Variation of the energy release rate of three radial cracks spaced equally at 120° apart originating from a circular hole with the pure mechanical load

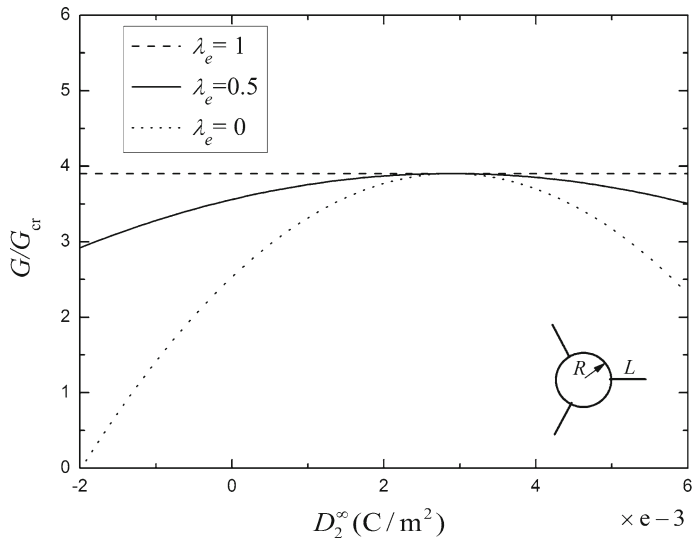

Fig. 8 Variation of the energy release rate of three radial cracks spaced equally at 120° apart originating from a circular hole with the applied electric load under a given mechanical loading $\sigma_{32}^{\infty} = 6$ MPa

In the same way, the effects of the number of cracks on the dimensionless intensity factor and the energy release rate under combined mechanical loading $\sigma_{32}^{\infty} = 6$ MPa and electric loading $D_2^{\infty} = 2\text{e} - 3$ C/m^2 for the case of star-shaped cracks are also plotted in Figs. 10 and 11, respectively, and similar results can be found. The difference is that the dimensionless intensity factor (Fig. 3) and the energy release rate (Fig. 6) for the case of multiple cracks originating from a circular hole are smaller than those for a single crack when $n > 5$, while the dimensionless intensity factor (Fig. 10) and the energy release rate (Fig. 11) for the case of star-shaped cracks are smaller than those for a single crack when $n > 13$.

5 Conclusions

The complex variable method and the technique of conformal mapping have been applied to treat the anti-plane problem of multiple cracks originating from a circular hole in an infinite piezoelectric solid by taking the effect of dielectric permittivity into consideration. This work is focused on the study of analytic solutions

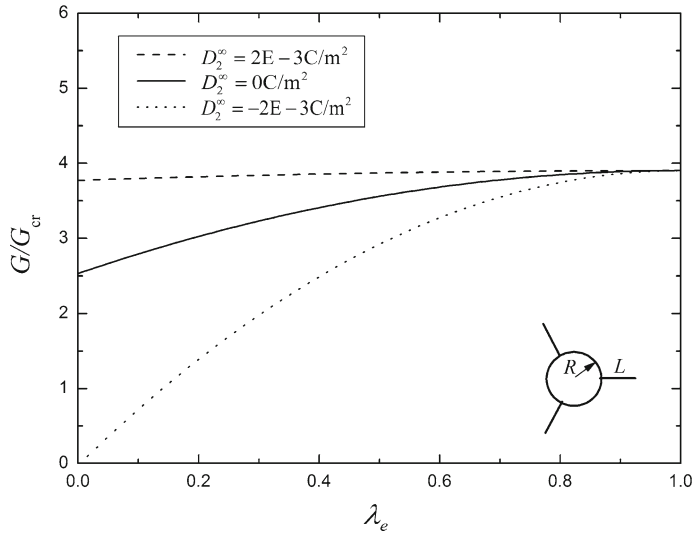

Fig. 9 Variation of the energy release rate of three radial cracks spaced equally at 120° apart originating from a circular hole with the parameter λ_e under a given mechanical loading $\sigma_{32}^{\infty} = 6$ MPa

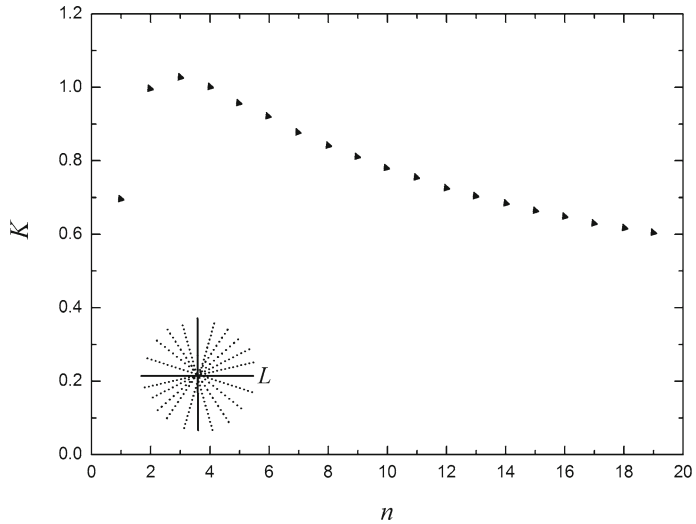

Fig. 10 Variation of K with the number of cracks n

of the field intensity factors and the energy release rate. Under some special limiting cases, the present results can be degenerated into the pervious ones, e.g., the Griffith crack, two symmetrical edge cracks and a single edge crack originating from a circular hole. And the results also provide new exact solutions for some more complicated defects including three radial spaced equally at 120° apart originating from a circular hole, four radial spaced equally at 90° apart originating from a circular hole, cross-shaped crack, star-shaped cracks, etc. Moreover, some valuable solutions of the stress intensity factor available in the previous literature can be taken as special cases of this paper. A comparison with the finite element method shows the accuracy and efficiency of the present method. Numerical examples are then provided to show the effect of the ratio of cracks length to hole-radius and the number of cracks on the dimensionless field intensity factors and the energy release rate under different loading conditions. In summary, the following conclusions can be drawn: (a) The increase in the crack length easily leads to the failure of materials. (b) The piezoelectric material containing three radial cracks spaced equally at 120° apart originating from a circular hole is the easiest to fail for all cases of cracks originating from a circular hole under anti-plane loadings. (c) The piezoelectric material containing two cracks or four cracks emanating from a circular hole is easier to fail than the material with a single crack originating from a circular hole. (d) If there exist multiple cracks ($n \geq 3$) originating from a circular hole

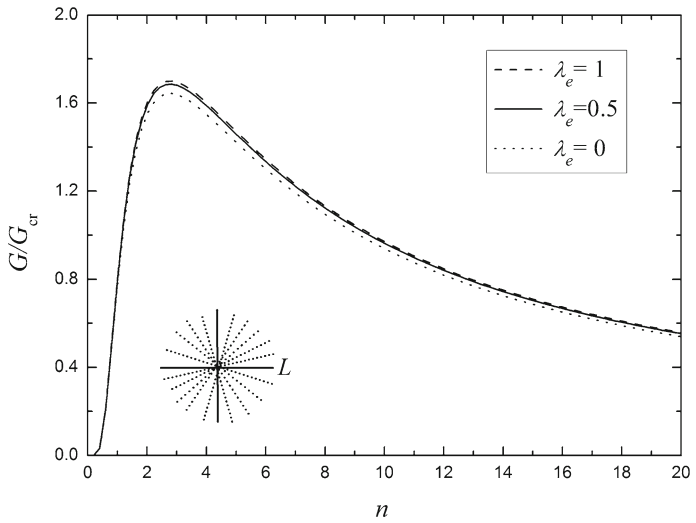

Fig. 11 Effect of the number of crack on the energy release rate of star-shaped cracks under combined mechanical loading $\sigma_{32}^{\infty} = 6$ MPa and electric loading $D_2^{\infty} = 2\text{e} - 3$ C/m^2

in piezoelectric materials, an increase in the number of cracks can enhance the reliability of this material. (e) Mechanical loading always promotes crack growth. Besides, for an impermeable crack or a semi-permeable crack under a given mechanical load, the negative electric field always impedes crack growth, while the positive electric field can either promote or retard crack propagation, which is dependent on both the strengths of the applied electric field and the level of the mechanical load. For a permeable crack under combined mechanical and electric loadings, the energy release rate is dependent on only the mechanical loading. (f) For a fixed mechanical loading, a negative electric loading is generally prone to inhibit the crack extension rather than a positive one.

Acknowledgments The authors thank the support from the National Natural Science Foundation of China (10932001 and 10761005) and the Scientific Research Key Program of Beijing Municipal Commission of Education (No. KZ201010005003). The authors are also grateful for valuable comments and suggestions from the anonymous referees for improvements of this paper.

References

1. Pak, Y.E.: Linear electroelastic fracture mechanics of piezoelectric materials. Int. J. Fract. **54**, 79–100 (1992)
2. Suo, Z., Kuo, C.M., Barnett, D.M., Willis, J.R.: Fracture mechanics for piezoelectric ceramics. J. Mech. Phys. Solids **40**, 739–765 (1992)
3. Sosa, H.: On the fracture mechanics of piezoelectric solids. Int. J. Solids Struct. **29**, 2613–2622 (1992)
4. Shindo, Y., Narita, F., Tanaka, K.: Electroelastic intensification near anti-plane shear crack in orthotropic piezoelectric ceramic strip. Theor. Appl. Fract. Mech. **25**, 65–71 (1996)
5. Shindo, Y., Tanaka, K., Narita, F.: Singular stress and electric fields of a piezoelectric ceramic strip with a finite crack under longitudinal shear. Acta Mech. **120**, 31–45 (1997)
6. Yang, F.Q., Kao, I.: Crack problem in piezoelectric materials: general anti-plane mechanical loading. Mech. Mater. **31**, 395–406 (1999)
7. Zhao, M.H., Shen, Y.P., Liu, G.N., Liu, Y.J.: Crack analysis in semi-infinite transversely isotropic piezoelectric solid. II. Penny-shaped crack near the surface. Theor. Appl. Fract. Mech. **32**, 233–240 (1999)
8. Gao, C.F., Wang, M.Z.: A permeable interface crack between dissimilar thermopiezoelectric media. Acta Mech. **149**, 85–95 (2001)
9. Suzuki, T., Sasaki, T., Hirashima, K., Kimura, K.: Analyses of isotropic piezoelectric materials with multilayered elliptical inclusion under out-of-plane shear loadings. Acta Mech. **179**, 211–225 (2005)
10. Hao, T.H., Shen, Z.Y.: A new electric boundary condition of electric fracture mechanics and its applications. Eng. Fract. Mech. **47**, 793–802 (1994)
11. Li, X.F., Lee, K.Y.: Electroelastic behavior of a rectangular piezoelectric ceramic with an antiplane shear crack at arbitrary position. Euro. J. Mech. A/Solids **23**, 645–658 (2004)
12. Li, X.F., Lee, K.Y.: A piezoelectric material with a periodic distribution of slant mode-III cracks. Mech. Mater. **37**, 189–200 (2005)
13. Zhang, T.Y., Gao, C.F.: Fracture behaviors of piezoelectric materials. Theor. Appl. Fract. Mech. **41**, 339–379 (2004)

14. Zhong, X.C., Li, X.F.: Closed-form solution for two collinear cracks in a piezoelectric strip. Mech. Res. Comm. **32**, 401–410 (2005)
15. Dyka, E., Rogowski, B.: Fundamental solutions in piezoelectricity. Penny-Shaped Crack Solution. Int. J. Press. Vess. Pip. **83**, 512–524 (2006)
16. Wang, Y.J., Gao, C.F.: The mode III cracks originating from the edge of a circular hole in a piezoelectric solid. Int. J. Solids Struct. **45**, 4590–4599 (2008)
17. Zhou, Z.G., Wang, B., Cao, M.S.: The behavior of permeable multi-cracks in a piezoelectric material. Mech. Res. Comm. **30**, 395–402 (2003)
18. Zhou, Z.G., Guo, Y., Wu, L.Z.: The behavior of three parallel non-symmetric permeable mode-III cracks in a piezoelectric material plane. Mech. Res. Comm. **36**, 690–698 (2009)
19. Zhou, Z.G., Zhang, P.W., Li, G.Q.: Interactions of multiple parallel symmetric permeable mode-III cracks in a piezoelectric material plane. Eur. J. Mech. A/Solids **28**, 728–737 (2009)
20. Zhou, Z.H., Xu, X.S., Leung, A.Y.T.: The mode III stress/electric intensity factors and singularities analysis for edge-cracked circular piezoelectric shafts. Int. J. Solids Struct. **46**, 3577–3586 (2009)
21. Guo, J.H., Lu, Z.X., Han, H.T., Yang, Z.: Exact solutions for anti-plane problem of two asymmetrical edge cracks emanating from an elliptical hole in a piezoelectric material. Int. J. Solids Struct. **46**, 3799–3809 (2009)
22. Kuna, M.: Fracture mechanics of piezoelectric materials—Where are we right now? Eng. Fract. Mech. **77**, 309–326 (2010)
23. Bowie, O.L.: Analysis of an infinite plate containing radial cracks originating at the boundary of an internal circular hole. J. Math. Phys. **35**, 60–71 (1956)
24. Tada, H., Paris, P.C., Irwin, G.R.: The stress analysis of cracks handbook. Del Research Corporation, Hellertown, PA (1973)
25. Ouchterlony, F.: Stress intensity factors for the expansion loaded star crack. Eng. Fract. Mech. **8**, 447–448 (1976)
26. Wu, X.R., Carlsson, A.J.: Weight Functions and Stress Intensity Factor Solutions. Pergamon Press (1991)
27. Zhang, T.Y., Zhao, M.H., Tong, P.: Fracture of piezoelectric ceramics. Adv. Appl. Mech. **38**, 147–289 (2002)
28. McMeeking, R.M.: The energy release rate for a Griffith crack in a piezoelectric material. Eng. Fract. Mech. **71**, 1149–1163 (2004)
29. Shindo, Y., Watanabe, K., Narita, F.: Electroelastic analysis of a piezoelectric ceramic strip with a central crack. Int. J. Eng. Sci. **38**, 1–19 (2000)
30. McMeeking, R.M.: Towards a fracture mechanics for brittle piezoelectric and dielectric materials. Int. J. Fract. **108**, 25–41 (2001)
31. Xu, X.L., Rajapakse, R.K.N.D.: On a plane crack in piezoelectric solids. Int. J. Solids Struct. **38**, 7643–7658 (2001)
32. Wang, X.D., Jiang, L.Y.: Fracture behavior of cracks in piezoelectric media with electromechanically coupled boundary conditions. Proc. R. Soc. London, Ser. A **458**, 2545–2560 (2001)
33. Wang, X.D., Jiang, L.Y.: The nonlinear fracture behavior of an arbitrarily oriented dielectric crack in piezoelectric materials. Acta Mech. **172**, 195–210 (2004)
34. Dascalu, C., Homentcovschi, D.: An intermediate crack model for flaws in piezoelectric solids. Acta Mech. **154**, 85–100 (2002)
35. Wang, B.L., Mai, Y.W.: On the electrical boundary conditions on the crack surfaces in piezoelectric ceramics. Int. J. Eng. Sci. **41**, 633–652 (2003)
36. Chiang, C.R., Weng, G.J.: Nonlinear behavior and critical state of a penny-shaped dielectric crack in a piezoelectric solid. ASME, J. Appl. Mech. **74**, 852–860 (2007)
37. Schneider, G.A., Felten, F., McMeeking, R.M.: The electrical potential difference across cracks in PZT measured by Kelvin Probe Microscopy and the implications for fracture. Acta Mater. **51**, 2235–2241 (2003)
38. Kwon, S.M.: On the dynamic propagation of an anti-plane shear crack in a functionally graded piezoelectric strip. Acta Mech. **167**, 73–89 (2003)
39. Zhong, X.C., Li, X.F.: Closed-form solution for an eccentric anti-plane shear crack normal to the edges of a magnetoelectroelastic strip. Acta Mech. **186**, 1–15 (2006)
40. Barnett, D.M., Lothe, J.: Dislocations and line charges in anisotropic piezoelectric insulators. Physica Status Solidi (b) **67**, 105–111 (1975)
41. Sih, G.C.: Stress distribution near internal crack tips for longitudinal shear problems. ASME, J. Appl. Mech. **32**, 51 (1965)
42. Pak, Y.E.: Crack extension force in a piezoelectric material. ASME, J. Appl. Mech. **57**, 647–653 (1990)